Position-independent self-adaptive wireless power transfer: topology, modeling, and design

David West [ID], Jinqun Ge [ID] and Guoan Wang [ID]

Department of Electrical Engineering, University of South Carolina, Columbia, SC, USA

Abstract

Wireless power transfer (WPT) is an emerging technology with many promising applications where transmitting power via wired connections is undesirable. However, near-field WPT between magnetically coupled inductors is highly susceptible to positional changes, with power transfer efficiency (PTE) suffering if the coils are misaligned. To combat this effect, many position-independent, self-adaptive, inductive WPT schemes have been developed. Recent work indicates that it is possible to passively achieve high PTE across the operating range with nonlinear capacitors. In this work, the functionality of nonlinear WPT circuits is investigated, and fundamental design equations are derived and validated. A simplified design procedure is proposed for the position-independent self-adaptive WPT using nonlinear capacitors, wherein the ideal capacitance is extracted for each coupling factor. The efficacy of the method is demonstrated with an experimental circuit. Future work in this area is also proposed.
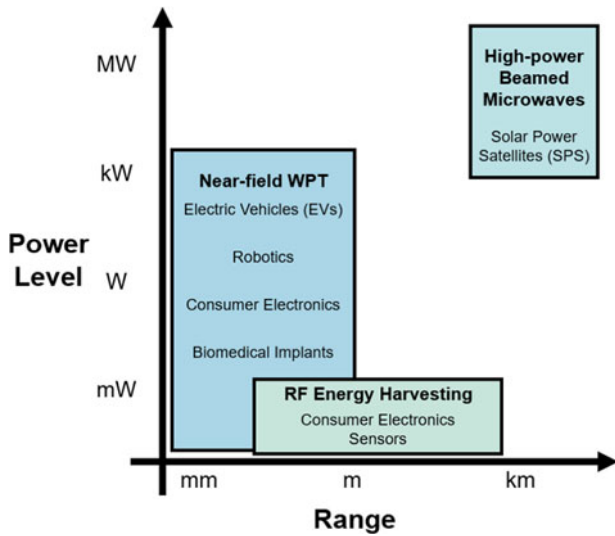
Introduction

Wireless power transfer (WPT) is an emerging technology permitting the transmission of electrical energy without a physical connection, useful in situations where supplying energy via a wired connection is impractical or undesirable. Relative power levels and transmission distances for three categories of WPT as described in [1] are shown in Fig. 1, with potential applications also shown for each. Near-field WPT operates at short ranges with varying power levels, depending on the application and size of the transmitting and receiving elements [2–6]. Radio frequency (RF) energy harvesting can operate at typical communication distances of meters to kilometers, but the power capability is limited, usually below the milliWatts (mW) level, due to the low energy levels of communication signals [7–9]. High-power, far-field transmission via beamed microwaves has also been studied. Proposed systems are intended to transmit Megawats (MW) of power from satellites in orbit down to the ground [10].

Near-field inductive WPT involves magnetic coupling between transmitting and receiving coils. An example of a two-coil inductive WPT setup is shown in Fig. 2. A power source excites a transmitting inductive coil. The magnetic field generated by the transmitter is coupled to a receiving coil, which connects to a load. The delivered power is highly sensitive to changes in the alignment of the coils [2]. As shown in Fig. 2, if the coils are too close together or not properly aligned along the same axis, the power transfer efficiency (PTE) is impacted. In an uncompensated system, the device receiving power must be accurately placed with respect to the transmitter to maximize energy transfer, which hampers practical usability.

Previous work in the literature has attempted to improve positional resilience and realize self-adaptive WPT with a variety of methods. It has been theoretically and experimentally shown that frequency tuning maintains stable PTE despite changes in coil position [11, 12], but such methods are limited at high frequencies due to Federal Communications Commission (FCC) bandwidth constraints [13]. In [14–16], switches are used to reconfigure an impedance-matching network of capacitors, which permits self-adaptive WPT at a stable frequency. Reference [12] also demonstrates active impedance-matching using a bank of dc-biased varactor diodes. However, the required control and matching circuits for either scheme considerably increase the complexity of the system [17]. As such, some passive designs have been proposed, including novel coil geometries [18, 19]. These avoid the complex circuit layouts of active designs, but strict physical constraints may preclude their application.

It has been shown in [17, 20] that it is possible to use varactors to create nonlinear resonators for self-adaptive WPT. In contrast to the dc-biased varactors used in [12], the proposed nonlinear WPT design automatically tunes the varactor capacitance based on the ac voltage level. Efficient power transfer can be passively maintained across the operating range using a relatively simple topology.

This paper thoroughly studies and validates position-independent, self-adaptive, nonlinear WPT technologies. It also discusses fundamental design aspects of WPT circuits

Figure 1. Applications of WPT, plotted in terms of relative transmission distance and power level. WPT = wireless power transfer.

Figure 2. Illustration of two-coil inductive WPT, depicting the sensitivity of PTE to positional changes. PTE = power transfer efficiency; WPT = wireless power transfer.

and introduces a simple methodology for designing the required nonlinearity in position-independent WPT systems; these design guidelines were followed when implementing the experimental WPT circuit. It then proposes ways to optimize the design further. Section "Linear WPT circuits" gives an overview of linear WPT circuits, discussing the theory behind positional sensitivity and the fundamental operating principle behind some self-adaptive schemes. Section "Nonlinear WPT design" discusses the nonlinear WPT circuit as well as the design procedure and its limitations. Section "Results and discussion" shows the measured results for the linear and nonlinear WPT circuits, with comparisons to simulation. Section "Conclusion and future work" concludes the paper and proposes a pathway for further study.

Linear WPT circuits

Network analysis

The general layout of a linear, two-coil inductive WPT circuit is shown in Fig. 3. It comprises a transmitting loop and a receiving loop, both of which are RLC resonators. The topology shown consists of two series resonators and is often termed a series–series (SS) circuit; other topologies exist with parallel resonators as well [17].

The circuit is driven on the transmitting side via the voltage source V_{in}, which can be modeled alongside an internal resistance R_1. This source takes the place of an RF power circuit that would be used to inject the voltage in a practical system. For the purposes of this study, PTE calculations are based purely on the V_{in} and resistance values.

The receiving side consists of a simple linear resistance R_2 to function as the load. The input impedance of the load in a practical setup (e.g., a rectifying circuit and a battery) could be considered in the design of the resonator [17].

The coupling between the inductors is characterized as a mutual inductance M_{12}, which is shown in Fig. 1. From [17], this quantity can be expressed in terms of the coil inductances and the coupling factor, k, as follows:

$$M_{12} = k\sqrt{L_1 L_2}. \tag{1}$$
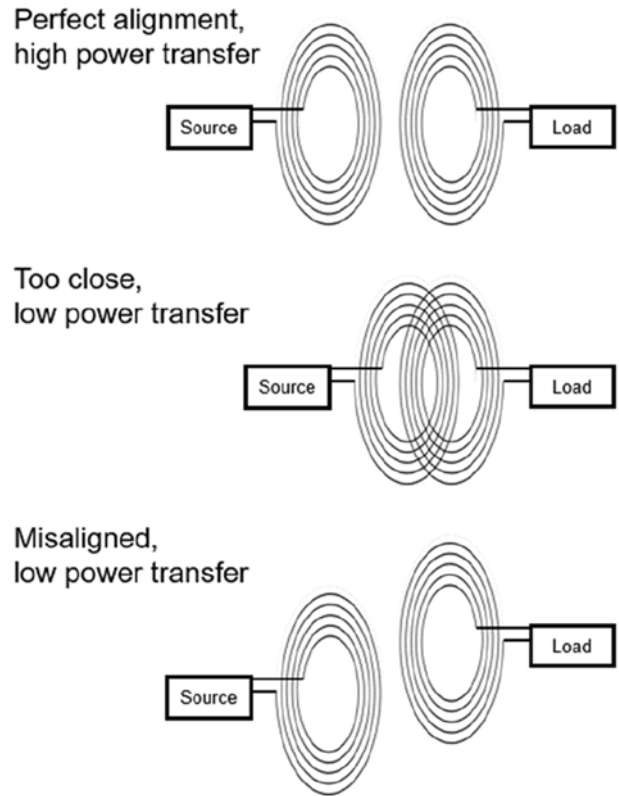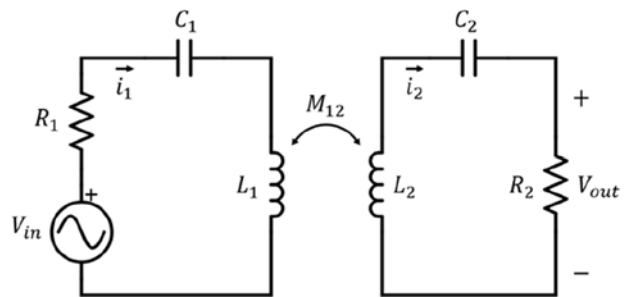
Figure 3. Typical topology of a linear series-series two-coil inductive WPT circuit. WPT = wireless power transfer.

The coupling factor is a convenient measure of the coupling strength, independent of the inductance values and varying between 0 and 1. As the inductors become more tightly coupled due to a higher amount of shared magnetic flux, the coupling factor increases. A higher coupling factor corresponds to a smaller distance between the coils and low angular or lateral misalignment. Conversely, the coupling factor decreases as the inductors become more loosely coupled due to lower shared magnetic flux. A low coupling factor corresponds to a greater distance between the coils or greater misalignment.

To maximize power delivery to the load, the loops are matched with $R_1 = R_2 = R$, $C_1 = C_2 = C$, and $L_1 = L_2 = L$, and the circuit is operated at the resonance frequency

$$\omega_0 = 2\pi f_0 = \frac{1}{\sqrt{LC}}. \tag{2}$$

While the transmitting and receiving circuits will not always be the same in practice, this condition is required for maximal power delivery to the load. If the circuits are not identical and additional resistances or reactances cannot be added to match the receiver to the transmitter, the maximum achievable power transfer will be reduced. For the purposes of this discussion, we assume that the transmitting and receiving loops are matched.

The PTE can be used as a figure of merit by comparing the power P_{out} realized across R_2 to the maximum possible power P_{av} that the source can deliver to a matched load [17]. For the WPT circuit in Fig. 1, the PTE is

$$PTE = \frac{P_{out}}{P_{av}} = \frac{V_{out}^2/R_2}{V_{in}^2/4R_1}. \tag{3}$$

Note that PTE is not the ratio of output to total input power; it is instead a measure of power delivery. These two different principles of efficiency versus power delivery are discussed in [3]. In the case of maximum power delivery, the impedance match described above would result in equal power dissipation in R_1 and R_2, or a PTE of 100%. However, energy efficiency expressed as P_{out}/P_{in} would be 50%, because the total input power is double the power delivered to R_2.

In Fig. 4, the coupled inductors are substituted with an equivalent T-junction, which incorporates the mutual inductance value M_{12} [21]. This configuration can be solved using standard network analysis procedures.

Kirchhoff's voltage and current laws can then be used to find the output voltage across R_2,

$$V_{out} = i_2 R_2 = \frac{Z_M V_{in} R_2}{Z_M (Z_1 + Z_2) + Z_1 Z_2}, \tag{4}$$

where

$$\begin{aligned} Z_1 &= R_1 + 1/j\omega C_1 + j\omega (L_1 - M_{12}) \\ Z_2 &= R_2 + 1/j\omega C_2 + j\omega (L_2 - M_{12}) \\ Z_M &= j\omega M_{12} \end{aligned} . \tag{5}$$

Equations (3–5) can be used to calculate the PTE. Figure 5 shows the result of a sweep of the coupling factor at the resonance frequency for an arbitrary example circuit. The PTE is maximized at a single coupling factor and rapidly drops off in either direction. The coupling factor with peak PTE is typically referred to as the "critical coupling factor" and can be indicated by k_c. The maximum of equation (4) may be found by taking the derivative with respect to k, which yields a closed-form expression for
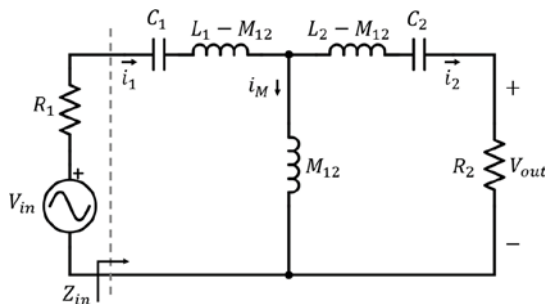

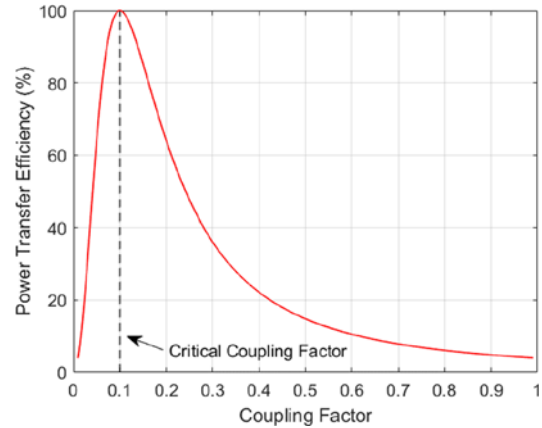**Figure 4.** Equivalent T-junction model of the WPT circuit. WPT = wireless power transfer.

Figure 5. Example PTE vs. coupling factor characteristic for an arbitrary WPT circuit at a single frequency. PTE = power transfer efficiency; WPT = wireless power transfer.
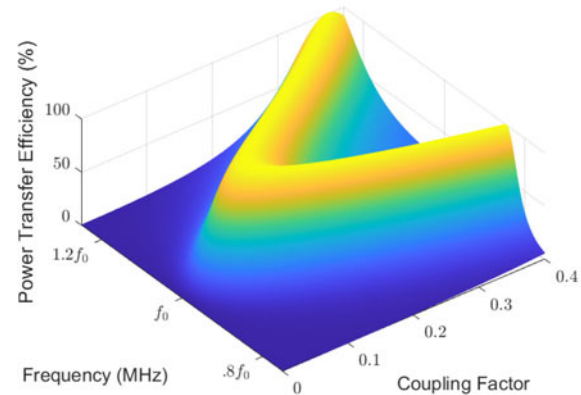

Figure 6. Result from sweeping both frequency and coupling factor for an arbitrary WPT circuit, displaying frequency split. WPT = wireless power transfer.

k_c [11]. After simplification, the critical coupling factor becomes the reciprocal of the WPT circuit's quality factor Q,

$$k_c = \frac{1}{Q} = R\sqrt{\frac{C}{L}}. \tag{6}$$

With no compensating elements or circuitry, the WPT circuit achieves maximum PTE at its resonant frequency with this single coupling factor. Because the coupling factor is a function of position, the circuit would have the highest power transfer for only a particular range of receiver locations and orientations relative to the transmitter. This is impractical, as the user would be required to accurately position the receiving element to ensure acceptable performance. For most situations, it is more desirable to maintain a high PTE for an extensive range of coupling factors.

Overcoupled region

The result in Fig. 5 is a coupling factor sweep at a single frequency—if the frequency is also swept alongside the coupling factor as shown in Fig. 6, a phenomenon known as "frequency split" appears [17]. This trait of WPT circuits is well-studied: above the critical coupling factor, in the area called the "overcoupled region," there are two frequencies at which PTE is still maximized.

The frequency split can be explained by examining the input impedance seen by the power source, depicted as Z_{in} in Fig. 4. When the circuit is at the resonant frequency ($f = f_0$) and the coils are critically coupled ($k = k_c$), Z_{in} is purely real and equal to R_2. The impedances of the reactive components cancel out, leaving only the load resistance. Because R_1 and R_2 are matched, PTE is maximized.

In the overcoupled region ($k > k_c$), the altered coupling factor results in a nonzero input reactance X_{in}, due to a shift of the mutual inductance M_{12}. At two specific frequencies for each coupling factor, the reactive elements cancel out again, bringing X_{in} back to 0. In these cases, Z_{in} is again purely real and equal to R_2, maximizing PTE.

The impedance-matching concept introduced by the frequency split phenomenon forms the basis of the operating principle behind the nonlinear circuit discussed in this work. In theory, altering capacitance or inductance would produce a similar result, with maximized PTE being achievable throughout the overcoupled region. More details may be found in section "Nonlinear WPT design".

Linear circuit design

The design of a nonlinear WPT circuit may begin with a linear circuit, which is enhanced by introducing the nonlinear components. This section discusses the considerations that went into the design of the linear WPT circuit used in this work.

Quality factor

The frequency split phenomenon indicates that within the overcoupled region, maximized PTE is possible if a compensation method is introduced. As such, the overcoupled region can be regarded as the operating range of the WPT circuit. In turn, the critical coupling factor represents the edge of the operating range [11]. The quality factor of the circuit, Q, directly affects the possible theoretical operating range of the WPT circuit due to the relationship shown in equation (6). Thus, higher quality factors are desirable, which can be achieved by lowering resistance and capacitance or increasing inductance. The flexibility to alter the quality factor may be limited by the application, where circuit parameters may be fixed.

There is an upper limit to the quality factor. Because compensation methods are not exact and errors will always exist, some tolerance is required. A high-Q circuit naturally has much tighter tolerances for every aspect of the design. Thus, a trade-off exists between robustness and range extension.

Inductor characterization

The inductive coils used in WPT are not typically purchased off-the-shelf and must be designed for the specific application. A natural shape for the coils is a flat spiral, which may satisfy physical constraints more easily than a cylindrical solenoid and can easily be modeled using a method from Maxwell's treatise, summarized in [22].

Maxwell's method models the mutual inductance between two circular, coaxial filamentary coils with radii a and b at a distance d, as shown in Fig. 7. The coils have zero angular misalignment, i.e., they lie on parallel planes. The mutual inductance, in Henries, is calculated as follows:

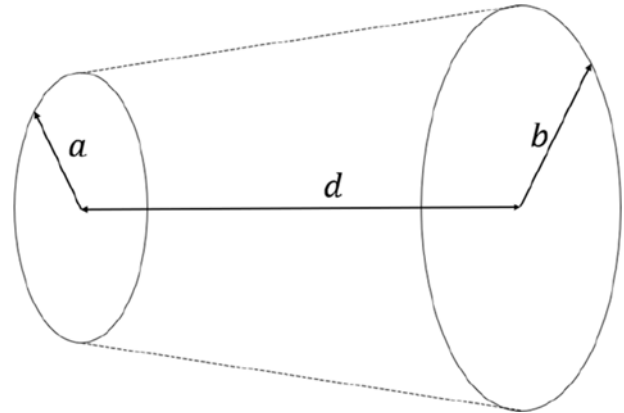$$M = -\mu_0 \sqrt{ab}\left(\left(k - \frac{2}{k}\right)F + \frac{2}{k}E\right), \tag{7}$$

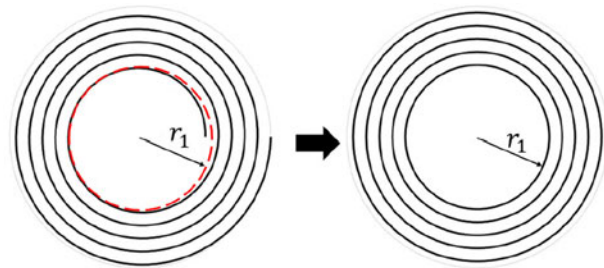**Figure 7.** Coaxial filamentary coils modeled by equation (7).

Figure 8. Modeling a spiral coil as a group of filamentary circles.

where F and E are elliptic integrals of the first and second kind to elliptic modulus k [22],

$$k = \frac{2\sqrt{ab}}{\sqrt{(a+b)^2 + d^2}}. \tag{8}$$

The elliptic integrals are well-studied and can be numerically calculated using built-in MATLAB functions. Equations (7) and (8) can be adapted to calculate the self-inductance of a single flat spiral coil by approximating each turn as an individual circular filament, as shown in Fig. 8. The radius of each circle is halfway between the start and end points of its respective turn.

The self-inductance, L, of an N-turn spiral coil is a summation of the mutual inductance between each pair of wire loops and the self-inductances of each turn. Each unique pair of loops is double-counted since the coils can be considered to be in series. The self-inductance can be calculated as follows:

$$L = \sum_{i}^{N} \sum_{j}^{N} M_{ij}, \tag{9}$$

where M_{ij} is the mutual inductance between turns i and j. Equations (7) and (8) may be rewritten as follows:

$$M_{ij} = -\mu_0 \sqrt{r_i r_j}\left(\left(k - \frac{2}{k}\right)F + \frac{2}{k}E\right),$$
$$k = \frac{2\sqrt{r_i r_j}}{\sqrt{(r_i + r_j)^2 + d^2}}. \tag{10}$$

The radii of the turns are expressed as r_i and r_j. The distance d is zero for most pairs $\{i,j\}$ since the turns lie on the

same plane. However, to account for the self-inductance of each turn (where $i = j$), the distance is set to the geometrical mean distance of that turn "from itself" [22]. In summary,

$$d = \begin{cases} 0 & i \neq j \\ r_w \exp{(-1/4)} & i = j \end{cases}, \quad (11)$$

where r_w is the radius of the actual wire used. This formulation allows for equation (10) to be used for the entire summation.

A similar summation can be used to calculate the mutual inductance between two spiral coils at a particular distance as follows:

$$M = \sum_{N_1}^{i} \sum_{N_2}^{j} M_{ij}. \quad (12)$$

In this case, i and j represent the loops on two separate inductors, so in general, the limits of the sums may be different. If the self-inductance of each spiral coil is known, the coupling factor can be extracted from mutual inductance using equation (1). Thus, the expected coupling factor for an inductor design may be estimated for a range of distances. The circuit parameters may be designed in tandem with the inductor geometry to estimate the theoretical maximum operating range of the self-adaptive WPT circuit.

Nonlinear WPT design

As previously mentioned, the frequency splitting phenomenon shown in section "Linear WPT circuits" forms the basis of the operating principle behind the self-adaptive WPT circuit in this work. It indicates that it is possible to use impedance-matching principles within the overcoupled region to maintain high PTE. It can be shown using network analysis that altering inductance or capacitance can work in an analogous manner to altering frequency. In practice, the altered capacitance may be realized using nonlinear capacitors. The design of the nonlinear WPT circuit is given here to demonstrate the proposed procedure.

Linear design

Based on the considerations given in section "Linear WPT circuits" as well as the available components, parameters for a linear WPT circuit were determined, as summarized in Table 1. A relatively low quality factor ($Q = 4.7$) was selected to improve the robustness of the circuit at the cost of potential operating range. With the resistance fixed at 50 Ω due to the output impedance of the signal generator, the linear capacitance and inductance had to be designed to achieve the desired quality factor. Note that the linear capacitance given in Table 1 is to be replaced entirely by the nonlinear capacitors. The power input level would typically be based on the system requirements. In this case, it could be selected freely, so 13.0 dBm was chosen based on the response of the varactors.

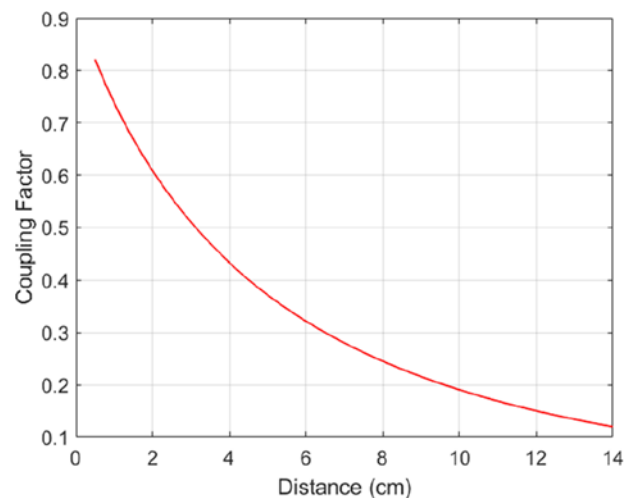**Table 1.** Wireless power transfer circuit parameters

Parameter	Value
Resistance, R	50 Ω
Inductance, L	43 μH
Linear capacitance, C	770 pF
Operating frequency, f	900 kHz
Input power, P	+13.0 dBm

The flat spiral inductors were wound using 10 turns of AWG 30 wire with an inner radius of 10 cm and an outer radius of 15 cm. The predicted coupling factor for a range of distances was calculated using equation (12) to verify that the operating range is reasonable. The result is plotted in Fig. 9. For a quality factor of ~5, the critical coupling factor is ~0.2, which corresponds to a separation of around 9 cm.

Nonlinear capacitor design

The design of the nonlinear capacitors involves determining the ideal values of capacitance at each coupling factor. Equations (3)–(5) were used to calculate the PTE for a sweep of distance and capacitance using the values in Table 1. The distance values were converted into a coupling factor using equation (12). The swept capacitance values apply to the capacitors on both loops (i.e., both C_1 and C_2 in Fig. 3). The results are plotted in Fig. 10.

There are two modes that appear. In the even mode, the capacitance decreases; in the odd mode, the capacitance increases. It can be seen from Fig. 10 that the even mode has a much shallower change in capacitance compared to the odd mode, which is easier to realize using off-the-shelf components. However, the width

Figure 9. Calculated coupling factor versus distance for the fabricated inductors.
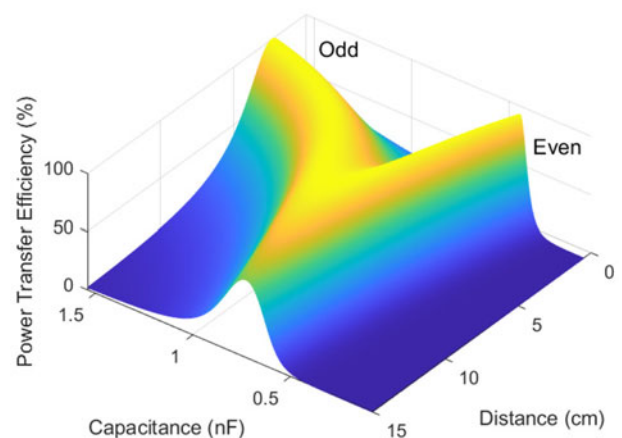
Figure 10. Result from sweeping coupling factor and capacitance for the WPT circuit defined by Table 1. WPT = wireless power transfer.

of the "ridge" in the odd mode is larger than in the even mode, meaning there is greater tolerance for changes in capacitance at a given distance. For this reason, the odd mode was selected for this design.

At each distance, the capacitance value in the odd mode that results in maximized PTE can be used to calculate the voltage across the capacitor in each loop. When PTE is maximized, the capacitor voltages are equal, so the same nonlinear design may be used for both capacitors. If the capacitance is then plotted as a function of voltage, the ideal capacitance–voltage (C–V) response is obtained, as shown in Fig. 11. The designed C–V response is also shown, which will be discussed next. If each linear capacitor is replaced with capacitors with the ideal C–V response, then maximized PTE can be retained across the operating range.

To realize the nonlinearity, varactor diodes are used, which have a well-documented relationship between capacitance and reverse bias voltage V_R [17],

$$C(V_R) = \frac{C_{jo}}{\left(1 + \frac{V_R}{V_{bi}}\right)^m}, \tag{13}$$

where C_{jo} is zero-bias junction capacitance, V_{bi} is built-in junction voltage, and m is the grading coefficient. This model is used in simulation program with integrated circuit emphasis (SPICE) simulators.

To prevent excessive distortion due to the current-blocking effects of the diode, a second varactor diode can be used in an antiseries configuration, as shown in Fig. 12. SPICE simulation can be used to obtain the C–V response of the antiseries pair. The applied voltag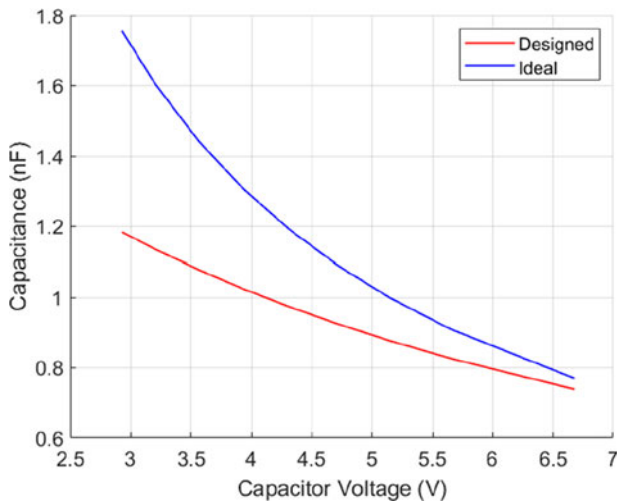e and resulting current are assumed to be dominated by their fundamental components, which are used to calculate the effective capacitance [20],
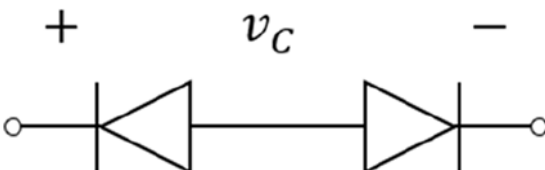
$$C_{eff} = \frac{I}{j\omega V}. \tag{14}$$

An off-the-shelf varactor diode is selected based on the approximate range of the ideal capacitance and voltage values. Next, SPICE simulation is used to characterize and design the C–V response when the selected varactor is implemented in antiseries configuration. More pairs can be added in series or parallel to tune the response.

For the designed C–V response shown in Fig. 11, five antiseries pairs of NTE618 are used in parallel. Due to the high steepness of the ideal curve, it is not practical to achieve a closer match, as a high number of varactors would be required. In this case, the chosen design is acceptable due to the higher tolerance offered by the low coupling factor. The designed response is closest to the ideal response at the critical coupling factor, where capacitor voltage is highest. The error increases as the circuit progresses deeper into the overcoupled region.

Results and discussion

The designed linear and nonlinear WPT circuits were simulated in Advanced Design System (ADS) and evaluated experimentally. Parasitic resistances $R_{loss} = 3\ \Omega$ were introduced based on the theoretical ac series resistance of the inductors, which was rounded up as a conservative estimate. It was found that this value yielded good agreement between the simulation and experiment. The nonlinear circuit was solved using the harmonic balance (HB) simulator in ADS. A diagram of the nonlinear circuit is shown in Fig. 13.

A picture of the experimental setup is shown in Fig. 14. An Agilent 33120A signal generator feeds the transmitting loop. A Tektronix TDS 2022C oscilloscope is used to capture the data. The coils were kept in angular alignment, and the transmitting coil was moved to vary the distance between them from 2 to 10 cm.

The node voltages V_1–V_4 marked in Fig. 13 were measured. The voltage across the load V_4 was used to calculate output power. The capacitor voltages were calculated from the node voltages (V_1 and V_2 for C_1 and V_3 and V_4 for C_2), and the currents in each loop were determined using Ohm's law. The signal generator was modeled as a voltage source with an internal resistance of 50 Ω capable of transmitting 13.0 dBm to a matched load, since the voltage "behind" the internal resistance could not be measured. This assumption was used to determine the current in the transmitting loop, i_1. The capacitor voltages and loop currents were used to determine the effective capacitance of the nonlinear capacitors.

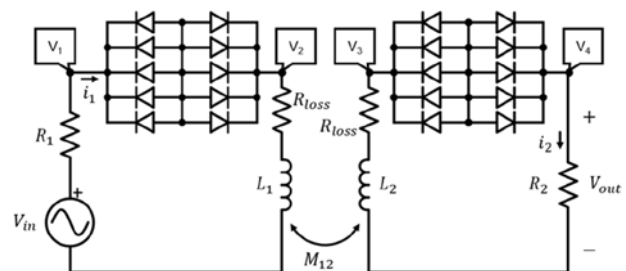

Figure 11. Ideal and designed C–V responses.

Figure 12. A pair of varactor diodes in antiseries configuration.

Figure 13. Schematic of the nonlinear circuit, including loss resistance and nodes where voltage was measured.
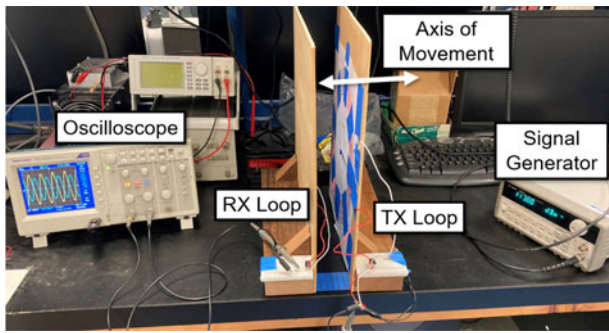
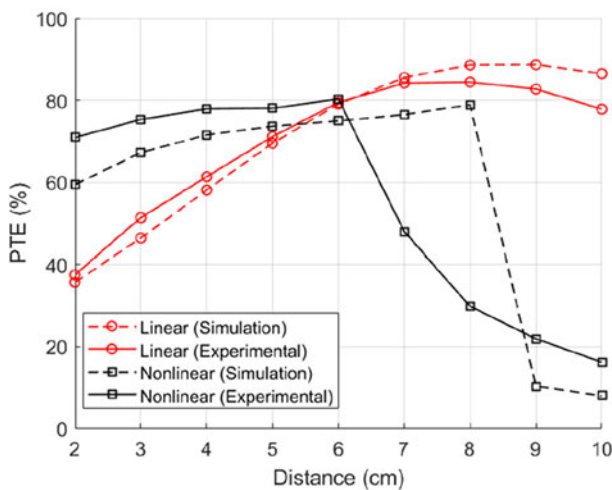**Figure 14.** Picture of the experimental setup.

Figure 15. Comparison of simulated and experimental results for PTE versus distance for linear and nonlinear WPT. PTE = power transfer efficiency; WPT = wireless power transfer.

Figure 16. Comparison of simulated and experimental results for effective capacitance versus distance, along with the ideal capacitance curve.

Similar procedures were followed in the ADS simulation to find PTE and effective capacitance.

Figure 15 shows the comparison of simulated and experimental PTE results for the linear and nonlinear WPT circuits. There is good agreement between the simulated and experimental linear circuit. Due to the relatively low quality factor, the range of the linear circuit is fairly broad; however, this will not always be the case, particularly for systems with lower resistance.

The simulated nonlinear circuit had a greater range than the experimental circuit, dropping off in PTE between 8 and 9 cm. The experimental nonlinear circuit displayed a remarkably similar trend, but the end of its operating range occurred at 6 cm. Between 2 and 6 cm, the experimental nonlinear circuit demonstrated improvement over the linear circuit while also outperforming the simulation. The discrepancy with the simulation can likely be attributed to the significant effects that initial conditions can have on the outcomes of a nonlinear system. The solution found by the HB simulation may be one of many possible stable solutions. By manipulating the initial conditions of the experimental circuit (such as with a startup circuit or by tuning the initial amplitude or frequency values), better performance may have been achievable at 8 and 9 cm. However, such measures lie outside the scope of this work and are suitable for further study.

Figure 16 shows the comparison of simulated and experimental effective capacitance values for the nonlinear WPT circuit between
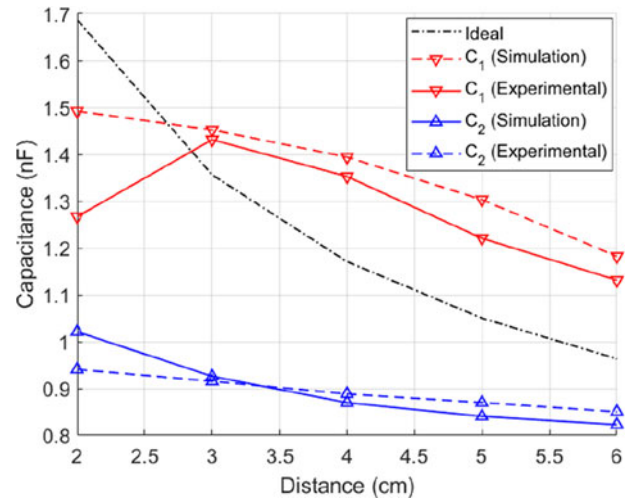
2 and 6 cm. A trace showing the calculated ideal capacitance for the odd mode is also shown. The experimental and simulated results are in good agreement overall. The transmitting-side capacitor C_1 was higher than the ideal capacitance for most of the operating range, while the receiving-side capacitor C_2 was lower across the entire range. The nonideal match due to the discrepancy between C_1 and C_2 resulted in a reduction of PTE. However, with C_1 and C_2 remaining near the ideal capacitance, the self-adaptive mechanism is achieved. Following the design principle proposed in this work and introducing the manipulation of initial conditions has the potential to achieve better results.

Conclusion and future work

In this work, fundamental analysis and design principles behind linear WPT circuits were presented, followed by a discussion of a proposed design procedure for position-independent self-adaptive WPT systems using nonlinear capacitors. An example nonlinear WPT circuit employing the described design principles was fabricated, achieving an optimum PTE with a large operating range within the overcoupled region and validating the findings in other work [17, 20]. Due to the low quality factor, the tolerance to shifts in quality factor for the linear circuit is relatively high, and the PTE of the nonlinear circuit is lower than that of the linear circuit beyond 6 cm. We also reiterate that the theoretical limit of the nonlinear circuit's operating range is defined by the critical coupling factor, so higher PTE for $k < k_c$ is not achievable. However, a linear WPT circuit with a higher quality factor would have a much steeper roll-off in PTE if critical coupling is not maintained. In this case, the nonlinear circuit would demonstrate a much larger operating range in comparison. Furthermore, the experiment demonstrated the efficacy of the design procedure, which obtains the ideal capacitance for each coupling factor to extract an ideal $C–V$ characteristic. Tuning or optimization may then be used to determine an arrangement of off-the-shelf components that satisfy the requirements.

Electrically tunable ferromagnetic thin-film technologies, as demonstrated in [23, 24], could enable the introduction of nonlinear inductors to the WPT system, which has the potential to further improve the PTE over a larger range. Current-dependent

inductors may introduce transient effects that lead to more reliable convergence on the desired high-PTE solution. Additionally, the nonlinearity of the inductors may reduce the steepness of the required $C-V$ curve, making it easier to achieve using off-the-shelf components.

Competing interests. The authors report no conflict of interest.

References

1. **Wu K, Choudhury D and Matsumoto H** (2013) Wireless power transmission, technology, and applications. *Proceedings of the IEEE* **101**, 1271–1275.
2. **Kurs A, Karalis A, Moffatt R, Joannopoulos JD, Fisher P and Soljacic M** (2007) Wireless power transfer via strongly coupled magnetic resonances. *Science* **317**, 83–86.
3. **Hui SYR, Zhong W and Lee CK** (2013) A critical review of recent progress in midrange wireless power transfer. *IEEE Transactions on Power Electronics* **29**, 4500–4511.
4. **Wei X, Wang Z and Dai H** (2014) A critical review of wireless power transfer via strongly coupled magnetic resonances. *Energies* **7**, 4316–4341.
5. **Li P and Bashirullah R** (2007) A wireless power interface for rechargeable battery operated medical implants. *IEEE Transactions on Circuits and Systems II: Express Briefs* **54**, 912–916.
6. **Li S and Mi CC** (2015) Wireless power transfer for electric vehicle applications. *IEEE Journal of Emerging and Selected Topics in Power Electronics* **3**, 4–17.
7. **Lu X, Wang P, Niyato D, Kim DI and Han Z** (2014) Wireless networks with RF energy harvesting: a contemporary survey. *IEEE Communications Surveys and Tutorials* **17**, 757–789.
8. **Jabbar H, Song YS and Jeong TT** (2010) RF energy harvesting system and circuits for charging of mobile devices. *IEEE Transactions on Consumer Electronics* **56**, 247–253.
9. **Walsh C, Rondineau S, Jankovic M, Zhao G and Popovic Z** (2005) A conformal 10 GHz rectenna for wireless powering of piezoelectric sensor electronics. In *Microwave Symposium Digest*, 143–146.
10. **Jaffe P and McSpadden J** (2013) Energy conversion and transmission modules for space solar power. *Proceedings of the IEEE* **101**, 1424–1437.
11. **Sample AP, Meyer DA and Smith JR** (2011) Analysis, experimental results, and range adaptation of magnetically coupled resonators for wireless power transfer. *IEEE Transactions on Industrial Electronics* **58**, 544–554.
12. **Heebl JD, Thomas EM, Penno RP and Grbic A** (2014) Comprehensive analysis and measurement of frequency-tuned and impedance-tuned wireless non-radiative power-transfer systems. *IEEE Antennas and Propagation Magazine* **56**, 131–148.
13. **Jang B-J, Lee S and Yoon H-G** (2012) HF-band wireless power transfer system: concept, issues, and design. *Progress in Electromagnetics Research* **124**, 211–231.
14. **Lee J, Lim Y-S, Yang W-J and Lim S-O** (2014) Wireless power transfer system adaptive to change in coil separation. *IEEE Transactions on Antennas and Propagation* **62**, 889–897.
15. **Beh TC, Kato M, Imura T, Oh S and Hori Y** (2013) Automated impedance matching system for robust wireless power transfer via magnetic resonance coupling. *IEEE Transactions on Industrial Electronics* **60**, 3689–3698.
16. **Bito J, Jeong S and Tentzeris MM** (2017) A novel heuristic passive and active matching circuit design method for wireless power transfer to moving objects. *IEEE Transactions on Microwave Theory & Techniques* **65**, 1094–1102.
17. **Abdelatty O, Wang X and Mortazawi A** (2019) Position-insensitive wireless power transfer based on nonlinear resonant circuits. *IEEE Transactions on Microwave Theory & Techniques* **67**, 3844–3855.
18. **Zhuang Y, Chen A, Xu C, Huang Y, Zhao H and Zhou J** (2019) Range-adaptive wireless power transfer based on differential coupling using multiple bi-directional coils. *IEEE Transactions on Industrial Electronics* **67**, 7519–7528.
19. **Niu W, Jiang J, Ye C and Gu W** (2022) Frequency splitting suppression in wireless power transfer using hemispherical spiral coils. *AIP Advances* **12**, 055016.
20. **Chai R and Mortazawi A** (2021) A position-insensitive wireless power transfer system employing coupled nonlinear resonators. *IEEE Transactions on Microwave Theory & Techniques* **69**, 1752–1759.
21. **Heebl JD** (2011) Development and characterization of a tunable resonant shielded loop wireless non-radiative power transfer system. M.S., School of Engineering, Univ. of Dayton.
22. **de Queiroz ACM** (2003) Mutual inductance and inductance calculations by Maxwell's method. UFRJ, Rio de Janeiro.
23. **Ge J, Wang T, Peng Y and Wang G** (2022) Electrically tunable microwave technologies with ferromagnetic thin film: recent advances in design techniques and applications. *IEEE Microwave Magazine* **23**, 48–63.
24. **Zhang Y, Ge J and Wang G** (2022) Enabling electrically tunable radio frequency components with advanced microfabrication and thin film techniques. *Journal of Central South University* **29**, 3248–3260.

David West received his B.S.E. in electrical engineering with a minor in computer science from the University of South Carolina, Columbia, SC, USA, in 2022. He has enrolled for graduate study at the Georgia Institute of Technology, Atlanta, GA, USA, starting in August 2022. He worked as an undergraduate research assistant at the University of South Carolina under Prof. Guoan Wang between October 2019 and May 2022. His research interests include wireless power transfer, nonlinear devices, and applied electromagnetics. Mr West was a recipient of the 2020 IEEE Microwave Theory and Techniques Society (IEEE MTT-S) Undergraduate/Pre-Graduate Scholarship. He was also awarded the Georgia Tech President's Fellowship in 2022 in support of his graduate study.

Jinqun Ge received the B.Sc. degree from Nanjing Normal University, Nanjing, China, in 2015 and the M.Sc. degree from Nanjing Normal University, Nanjing, China, in 2018. He is currently pursuing Ph.D. degree at the University of South Carolina, Columbia, SC, USA. His current research interests include microwave circuits and components, surface micromachining technologies, ferromagnetic and ferroelectric materials, and smart electrically tunable microwave components. Mr Ge was a recipient of the 2021 MTT-S Graduate Student Fellowship Award, the Best Student Paper Award in the 2020 IEEE MTT-S International Wireless Symposium, and Student Paper Honorable Mention in the IEEE 2020 Antenna and Propagation Symposium.

Guoan Wang received his Ph.D. in electrical and computer engineering from the Georgia Institute of Technology in 2006. He is currently a Professor and Director of the SMART Microwave and RF Technology Laboratory in the Department of Electrical Engineering at the University of South Carolina. He worked as an Advisory Scientist responsible for the development of on-chip mm-wave passives and wafer-level RF MEMS technologies in the IBM Semiconductor Research and Development Center from 2006 to 2011. His current research areas include reconfigurable RF and microwave electronics, novel materials/techniques for smart RF applications, MEMS/NEMS, sensors and sensing systems, wireless energy harvesting, and 3D integrated devices/system. Dr Wang's research work has produced over 140 papers in peer-reviewed journals and conference proceedings and one book (Smart RF Passive Components: Novel Materials, Techniques, and Applications, Artech House). He also has 51 granted US and international patents and 52 pending patent applications.

Dr Wang served as an Associate Editor of IEEE Microwave and Wireless Components Letters from 2013 to 2019 and is currently an Associate Editor of International Journal of RF and Microwave Computer-Aided Engineering. He is a member of the Technical Coordinating Committee for IEEE MTT TC-6 RF MEMS and Microwave Acoustics and chair of IEEE MTT TC-13 Microwave Control Materials and Devices. He has served in steering committees, technical program committees, and as session chairs of many IEEE conferences, including International Microwave Symposiums and IEEE Antennas and Propagation Symposium. Dr Wang is a recipient of the NSF Early Faculty Development (CAREER) Award in 2012, the IEEE Region 3 Outstanding Engineer Award in 2018, the USC Breakthrough Star Award in 2016, multiple IBM Invention Achievement Awards from 2008 to 2011, the NASA Tech Brief Award in 2007, and the Young Faculty Development Award from Southeastern Center for Electrical Engineering Education in 2013.